Three-dimension extracting transform

Xiangxiang Zhu[a], Haizhao Yang[b], Zhuosheng Zhang[a], Jinghuai Gao[c]

[a]*School of Mathematics and Statistics, Xi'an Jiaotong University, Xi'an 710049, China*
[b]*Department of Mathematics, Purdue University, West Lafayette, IN, USA, 47907*
[c]*National Engineering Laboratory for Offshore Oil Exploration, Xi'an 710049, China*

Abstract

In this paper, we consider three-dimensional parameter space, which is the time-frequency-chirprate (TFCR), to characterize the time-varying features of multi-component non-stationary signals. A highly concentrated TFCR representation, named as the three-dimension extracting transform (TET), is proposed based on instantaneous frequency (IF) and chirprate (CR) equations. The CRs and IFs can be jointly estimated via the TET, and spectral clustering algorithm is applied for component separation. To avoid the influence of the CR parameter on the IF identification, a nonlinear exponential transform of the IF and CR equations is introduced. We further give an TET reconstruction with theoretical analysis. By employing the TET, the signals crossing in the time-frequency domain can be well separated and robust IF estimation can be obtained. Numerical experiments on simulated signals demonstrate the effectiveness of the proposed method.

Keywords: Time-frequency-chirprate analysis, Synchrosqueezing transform, Chirplet transform, IF estimation, Overlapped signal detection

1. Introduction

Multi-component non-stationary signals, generally modeled as a superposition of amplitude-modulated and frequency-modulated (AM-FM) modes, are ubiquitous in science and engineering, e.g., seismic [1,2], astronomical [3], radar and sonar [4,5], biomedicine [6,7], and mechanical engineering [8,9]. The frequency is essential to describe such signals. In particular, time-frequency (TF) representations [4], which characterize how frequency contents evolve over time, provide a powerful tool for analyzing the multi-component non-stationary signals. The most two popular TF methods are probably the short-time Fourier transform (STFT) [10] and the continuous wavelet transform (CWT) [11], which serve as basic for signal detection. However, both transforms are limited by the Heisenberg uncertainty principle [4], failing to achieve a high-resolution signal representation both in time and in frequency simultaneously.

In the past decades, many works have been presented aiming at the high-resolution TF representation. The first attempt we think is the Wigner-Ville distribution (WVD) [4,12]. Although WVD is not constrained by the uncertainty principle, interference terms are introduced for multicomponent signals.

Email address: zhuxiagxiang@stu.xjtu.edu.cn (Xiangxiang Zhu)

Various smoothed versions of the WVD are developed to reduce the unwanted inferences [4,13,14], but the smoothing blurs the TF distribution. Another attempt, called the reassignment method (RM), dating back to the work by Kodera et al. [15] in the 1970s and further developed in [16], transfers the TF coefficients from the original position to the center of gravity of signal's energy distribution. The RM improves the energy concentration of the TF representation, but it lacks an explicit formula for signal reconstruction [17,18].

The empirical mode decomposition (EMD), proposed by Huang et al. [19], is a data-driven signal analysis technique to decompose the multi-component signal into a series of intrinsic mode functions (IMFs). By combining the EMD with the Hilbert transform, a sparse TF representation, i.e., the Hilbert-Huang transform (HHT) [19], is achieved by computing the IF of each IMF. Although the HHT proves to be interesting in many practical applications [19,20,21], the properties of EMD and its variants are not fully understood [22,23].

The synchrosqueezing transform (SST) is yet another approach to sharpen the TF representation. This method is initialized in [24] and further analyzed in [25]. By squeezing the TF coefficients into the IF trajectory in the frequency direction, the SST improves the TF readability; it still retains an explicit formula for signal recovery and gives new insights in understanding the principle of the EMD. Because of these properties, the SST has been widely studied. It has been proved that the SST is adapted to different transform frameworks, including the STFT-based SST [26], the synchrosqueezed curvelet transform [27], the synchrosqueezed wave packet transform [28], the synchrosqueezing S-transform [29], the chirplet-based SST [30], etc. The robust analysis and multivariate extensions of SST are presented in [31-35]. In spite of all these advances, one drawback associated with the SST in its original formulation is that it suffers from a low TF resolution when dealing with strongly AM-FM signals [18,36,37]. In this regard, many improvements of SST to better handle strong modulation signals are introduced, e.g., the demodulated SST [36,38], the high-order SST [37,39], the multiple squeezes transform [30,40], the time-reassigned SST [41].

Differing from the squeezing manner of the SST, the synchroextracting transform (SET) [42] obtains a sharpened TF representation by extracting the ridges of the STFT [43]. However, the TF ridge curves give a biased estimate for the true IFs when dealing with strong modulation signals [44]. To circumvent this drawback, Zhu et al. [43] proposed a chirplet synchroextracting transform, which retains the TF points satisfying an IF equation instead of the TF ridge. In addition, similar to the time-reassigned SST [41], a time-synchroextracting transform is also developed for transient signals analysis [45].

The TF post-processing methods introduced above have been widely used and adapted in many fields [1,9,20,21,31,35,39,45,46]. However, the performance of these methods depends on the basic assumption of separability, failing in the presence of crossed modes in the TF plane (see Fig. 5 for an illustration). To tackle this limitation, some attempts have been presented and they can be introduced in three aspects. The first one focuses on the modifications of RM [47,48] combining with the improved

ridge detection methods [49,50]. The modified RM methods correct the TF representation in the non-separable region partly, but no additional support can be used for distinguishing the different modes of the multi-component signal. In addition to TF methods, another two-dimension analysis is referred to as the time-chirprate (time-CR) representation, which mainly involves high-order ambiguity functions [51,52] and cubic phase functions [53,54]. For such methods, cross-terms are also introduced when multi-component signals are considered; at present, there is no sufficient study on sharpening the time-CR representation and how to solve the overlapped case in the time-CR plot. Instead of two-dimension signal representations, three-dimension representations (e.g. time-frequency-chirprate (TFCR)) [55,56] show great potential in processing multi-component non-stationary signals, since the intersected signals in the TF or time-CR domain frequently appear as separated in a high-dimensional space. However, how to obtain an accurate and concentrated three-dimensional signal representation is a challenging problem.

In this paper, we attempt to improve the resolution of the TFCR representation generated by the chirplet transform [43,55,57]. We propose a new transform, named as the three-dimension extracting transform (TET), to characterize the IF and CR information simultaneously based on IF and CR equations. The main contributions can be summarized:

1) We derive the IF and CR equations under the framework of the TFCR representation.
2) We propose a novel TET to obtain a sharpened three-dimensional representation by extracting the TFCR points satisfying the IF and CR equations, which extends the synchrosqueezed technology to three-dimension space.
3) An TET algorithm based on the exponential transform of the IF and CR equations is presented to realize the robust detection for IFs and CRs.
4) The TET breaks the separability limitation of the TF post-processing methods, and has a good performance in handling overlapped multi-component signals.

The remainder of the paper is organized as follows. In Section 2, the three-dimensional TFCR transform and its theoretical analysis are presented. In Section 3, we devote to the description of the proposed TET method. Experimental results and comparative studies are introduced in Section 4. Finally, the conclusions are drawn in Section 5.

2. Time-frequency-chirprate representation for multi-component non-stationary signal

2.1. Multi-component non-stationary signal

The multi-component non-stationary signal we considered in this paper is the AM-FM waves as

$$f(t) = \sum_{k=1}^{K} f_k(t) = \sum_{k=1}^{K} A_k(t) e^{j\phi_k(t)}, \tag{1}$$

where K is a positive integer representing the number of AM-FM components, $\sqrt{-1} = j$, $A_k(t) > 0$ and $\phi_k(t)$ are the instantaneous amplitude and instantaneous phase of the k-th component (or mode),

respectively. The first and the second derivatives of the phase, i.e., $\phi_k'(t)$, $\phi_k''(t)$, are referred to as the instantaneous frequency (IF) and chirprate (CR) of the signal.

The main aim of the multi-component non-stationary signal analysis is to get the instantaneous features of each component, mainly focusing on its instantaneous amplitude, IF and CR. In spite of the derivative relation between IF and CR, a joint representation that shows the IF and CR information simultaneously is great effective in multi-component signals analysis. Indeed, for $l \neq k$, $(\phi_l'(t), \phi_l''(t)) = (\phi_k'(t), \phi_k''(t))$ requires that these two components to be tangent in the TF plot, which is a more strict condition compared with the intersection in the TF/time-CR plane. Hence it is useful to show the signal representation in the TFCR domain, which can achieve good signal separation and estimation for the signals with cross-over frequencies.

2.2. Chirplet transform

The chirplet transform (CT) generalizes the STFT by using an extra CR parameter, which is defined as [30,55,57]

$$C_f^g(t,\omega,\beta) = \int_{-\infty}^{+\infty} f(\mu) g(\mu - t) e^{-\frac{j\beta(\mu-t)^2}{2}} e^{-j\omega(\mu-t)} d\mu, \tag{2}$$

where β is the CR parameter/variable, and $g(t)$ is a real and even window function. When $\beta \equiv 0$, this transform corresponds to the well known STFT. By introducing parameter β, CT maps the signal from the time domain to a three-dimensional space obtaining the TFCR representation.

Assume that around $\mu = t$ the mode $f_k(t) = A_k(t)e^{j\phi_k(t)}$ can be well approximated by its second-order local expansion:

$$f_k(\mu + t) \approx A_k(t) e^{j(\phi_k(t) + \phi_k'(t)\mu + \frac{1}{2}\phi_k''(t)\mu^2)}. \tag{3}$$

As the Gaussian window function $g(t) = \sigma^{-\frac{1}{2}} e^{-\frac{t^2}{2\sigma^2}}$ is employed, the CT result of the $f(t)$ under the hypothesis (3) is simple gaussian integral as follows:

$$\begin{aligned} C_f^g(t,\omega,\beta) &= \sum_{k=1}^{K} f_k(t) \int_{-\infty}^{+\infty} g(\mu) e^{\frac{-j(\beta-\phi_k''(t))\mu^2}{2}} e^{-j(\omega-\phi_k'(t))\mu} d\mu \\ &= \sum_{k=1}^{K} f_k(t) \sqrt{\sigma} \sqrt{\frac{2\pi}{1 + j\sigma^2(\beta - \phi_k''(t))}} \exp\left(-\frac{\sigma^2(\omega - \phi_k'(t))^2}{2(1 + j\sigma^2(\beta - \phi_k''(t)))} \right). \end{aligned} \tag{4}$$

In the strict sense, Equation (4) should be a approximate equality, but for convenience and illustrative purpose, an exact equality is given.

From (4), we can obtain the following theorem.

Theorem 1. *For the constant-amplitude linear frequency-modulated signals, if the window width in the CT is taken as a large enough value, then*

$$| C_f^g(t,\omega,\beta) |^2 = \sum_{k=1}^{K} A_k^2(t) \sigma \delta(\omega - \phi_k'(t)) \delta(\beta - \phi_k''(t)), \tag{5}$$

where $\delta(\cdot)$ is the Dirac delta function.

Proof For the constant-amplitude linear frequency-modulated signals, the approximation (3) is hold for any time internal, then expression (4) is true for any window's size σ. Let

$$C_{f_k}^g(t,\omega,\beta) = f_k(t)\sqrt{\sigma}\sqrt{\frac{2\pi}{1+j\sigma^2(\beta-\phi_k''(t))}}\exp\left(-\frac{\sigma^2(\omega-\phi_k'(t))^2}{2(1+j\sigma^2(\beta-\phi_k''(t)))}\right) = M_k(t,\omega,\beta)e^{j\Phi_k(t,\omega,\beta)},$$

then expression (4) can be reformulated as

$$C_f^g(t,\omega,\beta) = \sum_{k=1}^{K} M_k(t,\omega,\beta)e^{j\Phi_k(t,\omega,\beta)}. \tag{6}$$

The module of the CT is obtained by

$$\mid C_f^g(t,\omega,\beta) \mid^2 = \sum_{k=1}^{K} M_k(t,\omega,\beta)^2 + \sum_{k=1}^{K-1}\sum_{l=k+1}^{K} 2M_k(t,\omega,\beta)M_l(t,\omega,\beta)\cos(\Phi_k(t,\omega,\beta)-\Phi_l(t,\omega,\beta)).$$

For any $k \in \{1,2,\cdots,K\}$,

$$M_k(t,\omega,\beta)^2 = A_k(t)^2 2\pi\sigma\frac{1}{\sqrt{1+\sigma^4(\beta-\phi_k''(t))^2}}\exp\left(-\frac{\sigma^2(\omega-\phi_k'(t))^2}{1+\sigma^4(\beta-\phi_k''(t))^2}\right), \tag{7}$$

thus, for $\omega = \phi_k'(t)$, $\beta = \phi_k''(t)$, we have

$$M_k(t,\omega,\beta)^2 = A_k(t)^2 2\pi\sigma. \tag{8}$$

For $\omega = \phi_k'(t)$, $\beta \neq \phi_k''(t)$, we can obtain that

$$M_k(t,\omega,\beta)^2 = \frac{A_k(t)^2 2\pi\sigma}{\sqrt{1+\sigma^4(\beta-\phi_k''(t))^2}}, \tag{9}$$

then $M_k(t,\omega,\beta) \to 0$ when $\sigma \to \infty$.

For $\omega \neq \phi_k'(t)$, it also can obtain that $M_k(t,\omega,\beta) \to 0$ with $\sigma \to \infty$. Based on the three situations analyzed above, we can obtain the result (5), which finishes the proof.

Theorem 1 proves that, if a wide window is adopted, the CT has a perfect concentration in the frequency-chirprate (frequency-CR) plane for constant-amplitude linear frequency-modulated signals. In practical application, however, a wide window may cause an unsatisfactory result due to the approximation (3) is not true for a wide window in dealing with fast-varying signals [58], which are very common in many fields of practical interest, e.g., mechanical vibration [41], gravitational waves [59]. In this regard, a narrow window is required, but a narrow size diffuses the energy distribution of the CT.

Let us consider an example:

$$\begin{aligned} f(t) &= f_1(t) + f_2(t) + n(t), \\ f_1(t) &= \exp(-0.03t)\sin(2\pi(-90t^2+220t)), \\ f_2(t) &= (1+0.1\cos(20\pi t))\cos(2\pi(10\sin(2\pi t)+80t)), \end{aligned} \tag{10}$$

where $n(t)$ is a Gaussian noise and the SNR = 16 dB. The sampling frequency is 512 Hz, and time duration is [0 1]. The STFT of this test signal is illustrated in Fig. 1(a). Fig. 1 (b-c) display the

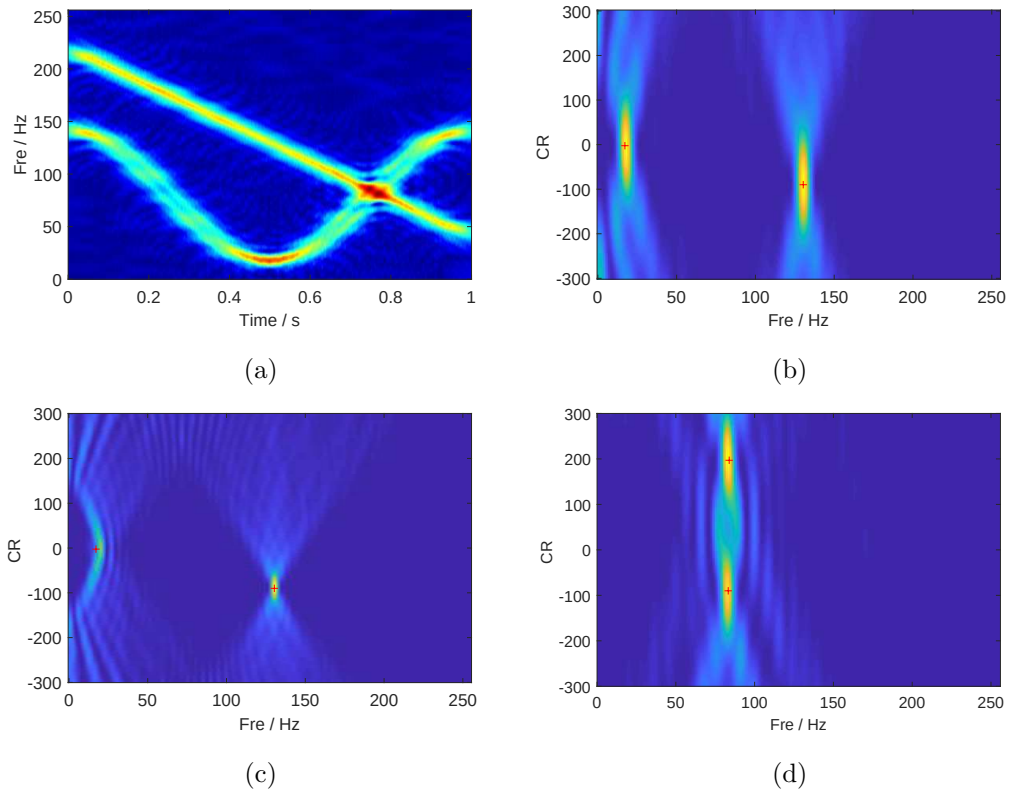

Figure 1: The STFT and CT slices for the test signal. (a) The STFT, (b) the CT slice of $t = 0.5$ s when window length is taken as 67 points, (c) the CT slice of $t = 0.5$ s when the window length is taken as 127 points, (d) the CT slice of $t = 0.76$ s when window length is taken as 67 points.

CT slices ($t = 0.5$ s) of this signal using different window lengths, where the red notes are the true instantaneous features of the signal. Obviously, a wide window concentrates the result of $f_1(t)$ but leads the energy distribution of $f_2(t)$ to deviating from the true value. A narrow window is preferred for $f_2(t)$, but it spreads the representation.

Furthermore, to discuss the separability of the TFCR representation, we assume the window $g(t)$ be such that $supp(\hat{g}) \subset [-\Delta, \Delta]$. For the well separated case in the TF domain, i.e., $\mid \phi_l'(t) - \phi_k'(t) \mid \geq 2\Delta$ for all $k, l \in \{1, 2, \cdots, K\}$, $t \in R$, they can be separated in the TFCR domain equally and the CR parameter can be simply set as presented in [43,57]. For the non-separable case, we suppose there exist two components (e.g., f_l, f_k) such that $\mid \phi_l'(t) - \phi_k'(t) \mid < 2\Delta$, $t \in [t_1, t_2]$, the TFCR representation also can separate them when they have different CRs. Theorem 2 shows the detail.

Theorem 2. *For the multi-component signal (1), suppose there exist two components (e.g., $f_l(t)$, $f_k(t)$) such that $\mid \phi_l'(t) - \phi_k'(t) \mid < 2\Delta$, $t \in [t_1, t_2]$, and $\sup_{t \in R} A_i(t) < \infty$, $i = l, k$, if $\mid \phi_l''(t) - \phi_k''(t) \mid > \frac{2\sqrt{1-\varepsilon^2}}{\sigma^2 \varepsilon}$ for $t \in [t_1, t_2]$, then we have*

$$\mid C_{f_i}^g(t, \omega, (\phi_l''(t) + \phi_k''(t))/2) \mid^2 < C\varepsilon, \ \omega \in [\phi_i'(t) - \Delta, \phi_i'(t) + \Delta], \ t \in [t_1, t_2], \ i = l, k, \tag{11}$$

where C is a positive constant, and $\varepsilon < 1$ is a small positive number.

Proof From (7), we have

$$\mid C_{f_i}^g(t,\omega,\beta)\mid^2 = A_i(t)^2 2\pi\sigma \frac{1}{\sqrt{1+\sigma^4(\beta-\phi_i''(t))^2}} \exp\left(-\frac{\sigma^2(\omega-\phi_i'(t))^2}{1+\sigma^4(\beta-\phi_i''(t))^2}\right).$$

For $i = l, k$, it is easy to obtain that

$$\mid C_{f_i}^g(t,\omega,(\phi_l''(t)+\phi_k''(t))/2)\mid^2 = A_i(t)^2 2\pi\sigma \frac{1}{\sqrt{1+\sigma^4(\frac{\phi_l''(t)-\phi_k''(t)}{2})^2}} \exp\left(-\frac{\sigma^2(\omega-\phi_i'(t))^2}{1+\sigma^4(\frac{\phi_l''(t)-\phi_k''(t)}{2})^2}\right).$$

Due to $\mid \phi_l''(t) - \phi_k''(t)\mid > \frac{2\sqrt{1-\varepsilon^2}}{\sigma^2\varepsilon}$, we have

$$\mid C_{f_i}^g(t,\omega,(\phi_l''(t)+\phi_k''(t))/2)\mid^2 \leq A_i(t)^2 2\pi\sigma \frac{1}{\sqrt{1+\sigma^4(\frac{\phi_l''(t)-\phi_k''(t)}{2})^2}} < A_i(t)^2 2\pi\sigma\varepsilon, \tag{12}$$

for $\omega \in [\phi_i'(t)-\Delta, \phi_i'(t)+\Delta]$, $t \in [t_1\ t_2]$. As $\sup_{t\in R} A_i(t) < \infty$, $i = l, k$, we can obtain the result (11), which finishes the proof.

It follows that $\mid C_{f_i}^g(t,\omega,(\phi_l''(t)+\phi_k''(t))/2)\mid^2 < \varepsilon \mid C_{f_i}^g(t,\phi_i'(t),\phi_i''(t))\mid^2$ when $\omega \in [\phi_i'(t)-\Delta, \phi_i'(t)+\Delta]$, $t \in [t_1, t_2]$, which in fact shows the separability of the modes $f_l(t)$ and $f_k(t)$ in the TFCR domain provided ε is a sufficiently small. A simple example is showed in Fig. 1 (a,d). This signal crosses in the TF plane while separates in the TFCR domain. From the Theorem 2, we also know that a large size σ used in the CT for linear frequency-modulated signals can help to distinguish the TF crossed components even with close CRs.

3. Three-dimension extracting transform

In this section, we consider how to sharpen the TFCR representation and to obtain the IF and CR information from the three-dimensional signal representation.

3.1. TET

One way to sharpen the TFCR representation is to detect the maximum in the frequency-CR domain for each time t [56,60]. But this method is easily influenced by the signal amplitude, and with limited generality. In the following, we will give an alternative to obtain a high concentration TFCR representation.

For the convenience of the following explanation, we consider the case of a monocomponent signal $f(t) = A(t)\exp(j\phi(t))$. The multicomponent signals can be handled similarly if all of modes are well separated in the TFCR domain. Under the assumption (3), the CT of the monocomponent $f(t)$ is given by

$$\begin{aligned} C_f^g(t,\omega,\beta) &= \int_{-\infty}^{+\infty} f(\mu)g(\mu-t)e^{-\frac{j\beta(\mu-t)^2}{2}}e^{-j\omega(\mu-t)}d\mu \\ &= f(t)\sqrt{\sigma}\sqrt{\frac{2\pi}{1+j\sigma^2(\beta-\phi''(t))}}\exp\left(-\frac{\sigma^2(\omega-\phi'(t))^2}{2(1+j\sigma^2(\beta-\phi''(t)))}\right). \end{aligned} \tag{13}$$

From (13), we can obtain that

$$\frac{\partial}{\partial\omega}C_f^g(t,\omega,\beta) = C_f^g(t,\omega,\beta)\left(-\frac{\sigma^2(\omega-\phi'(t))}{1+j\sigma^2(\beta-\phi''(t))}\right). \tag{14}$$

Then the set of points $\omega = \phi'(t)$ satisfies

$$\Re\left\{\frac{\frac{\partial}{\partial\omega}C_f^g(t,\omega,\beta)}{C_f^g(t,\omega,\beta)}\right\} = 0, \quad \text{for } \mid C_f^g(t,\omega,\beta)\mid > \gamma, \tag{15}$$

where the parameter $\gamma > 0$ is a hard threshold on $\mid C_f^g(t,\omega,\beta)\mid$ to overcome the shortcoming that $\mid C_f^g(t,\omega,\beta)\mid \approx 0$, and $\Re\{\cdot\}$ denotes the real part of complex number. Equation (15) is called the IF equation because the $\omega = \phi'(t)$ is its solution.

Similarly, we can also derive the CR equation, i.e., the set of points $\beta = \phi''(t)$ satisfies

$$\Im\left\{\frac{C_f^g(t,\omega,\beta)^2}{\frac{\partial^2}{\partial\omega^2}C_f^g(t,\omega,\beta)\times C_f^g(t,\omega,\beta) - \frac{\partial}{\partial\omega}C_f^g(t,\omega,\beta)^2}\right\} = 0, \tag{16}$$

for $\mid \frac{\partial^2}{\partial\omega^2}C_f^g(t,\omega,\beta)\cdot C_f^g(t,\omega,\beta) - \frac{\partial}{\partial\omega}C_f^g(t,\omega,\beta)^2 \mid > \gamma$, where $\Im\{\cdot\}$ is the imaginary part of complex number.

Combining (15) and (16), the points $(\phi'(t),\phi''(t))$ can be estimated by solving IF and CR equations:

$$\begin{cases}\hat{\omega}(t,\omega,\beta) := \Re\{\frac{\frac{\partial}{\partial\omega}C_f^g(t,\omega,\beta)}{C_f^g(t,\omega,\beta)}\} = 0,\\ \hat{\beta}(t,\omega,\beta) := \Im\{\frac{C_f^g(t,\omega,\beta)^2}{\frac{\partial^2}{\partial\omega^2}C_f^g(t,\omega,\beta)\times C_f^g(t,\omega,\beta) - \frac{\partial}{\partial\omega}C_f^g(t,\omega,\beta)^2}\} = 0.\end{cases} \tag{17}$$

Based on equations (17), a novel TFCR representation called the three-dimension extracting transform (TET) is proposed, which is,

$$Te(t,\omega,\beta) = C_f^g(t,\omega,\beta)\delta(\hat{\omega}(t,\omega,\beta))\delta(\hat{\beta}(t,\omega,\beta)). \tag{18}$$

The TET extracts the TFCR points that satisfy the equations (17) and only few points are retained, which can improve the concentration of the representation effectively. Fig. 2 shows two TET results of the signal (10). Compared with the CT results presented in Fig. 1(b,d), the proposed TET obtains a concentrated frequency-CR representation, accurately detecting the instantaneous information at the given times.

It is worth noting that, the performance of the TET depends on the equations (17) because they determine the accuracy of the IF and CR detection. More effective exploration, instead of the equations (17), should be considered in the future to make the TET more precise and robust.

3.2. Algorithm implementation

In this section, we discuss the algorithm implementation for the TET. Indeed, the key step of the TET algorithm is to obtain the solutions of the IF and CR equations.

A problem about the IF equation (15) is that the CR term influences its detection performance. Since $\hat{\omega}(t,\omega,\beta) = \Re\{\frac{\frac{\partial}{\partial\omega}C_f^g(t,\omega,\beta)}{C_f^g(t,\omega,\beta)}\} = \frac{-\sigma^2(\omega-\phi'(t))}{1+\sigma^4(\beta-\phi''(t))^2}$, the denominator $(\beta-\phi''(t))^2$ leads the value of $\mid \hat{\omega}(t,\omega,\beta)\mid$

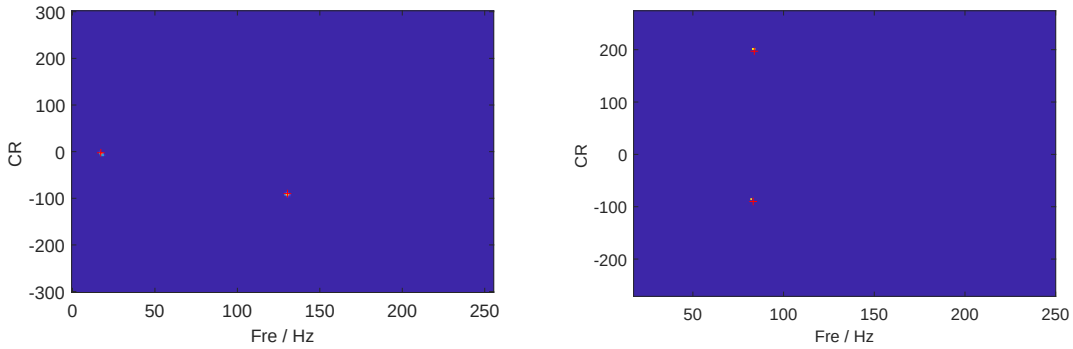

Figure 2: TET results. (a) The TET result at $t = 0.5$ s, (b) the TET result at $t = 0.76$ s.

to near zero when the value of $(\beta - \phi''(t))^2$ toward infinity. As presented in Fig. 3(a), the exponential expression of the $\hat{\omega}$, i.e. $\exp(-\hat{\omega}^2)$, has a large value when $\mid \beta - \phi''(t) \mid > 200$. Therefore, it is inevitable to induce the detection error for the IF solution $\omega = \phi'(t)$ if we directly employ the criterion (15).

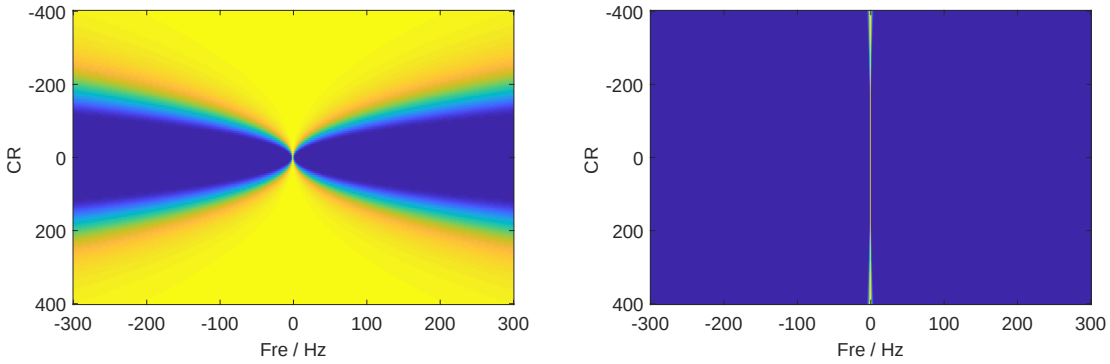

Figure 3: An illustration of the influence of the CR parameter on the IF equation. (a) The plot of $\exp(-\frac{\sigma^4\omega^2}{(1+\sigma^4\beta^2)^2})$, (b) the plot of the $\exp(-C_\omega^2\frac{\sigma^4\omega^2}{(1+\sigma^4\beta^2)^2})$, where $C_\omega = 800$.

To tackle the problem above, we can introduce a constant $C_\omega > 0$ to eliminate the effect of the CR term. Suppose $\phi''(t) \in [\beta_{min}\ \beta_{max}]$ for $t \in R$, then the quantity $(\beta - \phi''(t))^2$ is bounded if we also consider the parameter $\beta \in [\beta_{min}\ \beta_{max}]$. Based on that, we can take one constant C_ω such that $\frac{C_\omega^2\sigma^2}{1+\sigma^4(\beta-\phi''(t))^2} > 1$, and then the exponential expression $\exp(-{C_\omega}^2\hat{\omega}^2)$ concentrates along the $\omega = \phi'(t)$, as illustrated in Fig. 3(b). Therefore, it is easy to detect the points of $\omega = \phi'(t)$ based on the exponential transform of the IF equation as

$$\exp(-{C_\omega}^2\hat{\omega}(t,\omega,\beta)^2) > \tau, \tag{19}$$

where $\tau \in (0, 1]$ is a threshold.

For the CR equation (16), we can also use the exponential transform of the (16), which is $\exp(-{C_\beta}^2\hat{\beta}^2)$ (C_β is a positive constant), to pick up the points of $\beta = \phi''(t)$ because $\exp(-{C_\beta}^2\hat{\beta}^2)$ also concentrates along the $\beta = \phi''(t)$. Consequently, the intersection point of the exponential transform $\exp(-{C_\omega}^2\hat{\omega}^2)$ and $\exp(-{C_\beta}^2\hat{\beta}^2)$ corresponds to the solution of the equations (17), which can be implemented by finding the point (t, ω, β) such that

$$\exp(-{C_\omega}^2\hat{\omega}(t,\omega,\beta)^2)\exp(-{C_\beta}^2\hat{\beta}(t,\omega,\beta)^2) > \tau. \tag{20}$$

For more precise parameter estimation, $\frac{\partial}{\partial\omega}C_f^g(t,\omega,\beta)$ can be calculated by

$$\frac{\partial}{\partial\omega}C_f^g(t,\omega,\beta) = \frac{\partial}{\partial\omega}\left(\int_{-\infty}^{+\infty} f(\mu)g(\mu-t)e^{-j\beta(\mu-t)^2/2}e^{-j\omega(\mu-t)}d\mu\right) = -jC_f^{tg}(t,\omega,\beta), \tag{21}$$

where $C_f^{tg}(t,\omega,\beta)$ denotes the CT of $f(t)$ obtained by using the window function $tg(t)$. Similarly, for $\frac{\partial^2}{\partial\omega^2}C_f^g(t,\omega,\beta)$, we also have

$$\frac{\partial^2}{\partial\omega^2}C_f^g(t,\omega,\beta) = -C_f^{t^2g}(t,\omega,\beta), \tag{22}$$

where $C_f^{t^2g}(t,\omega,\beta)$ denotes the CT of $f(t)$ under the window function $t^2g(t)$. Combing (21)-(22), the IF and CR equations (17) can be rewritten as

$$\begin{cases} \hat{\omega}(t,\omega,\beta) = \Im\left\{\frac{C_f^{tg}(t,\omega,\beta)}{C_f^g(t,\omega,\beta)}\right\} = 0, \\ \hat{\beta}(t,\omega,\beta) = \Im\left\{\frac{C_f^g(t,\omega,\beta)^2}{{C_f^{tg}(t,\omega,\beta)}^2 - C_f^{t^2g}(t,\omega,\beta)\times C_f^g(t,\omega,\beta)}\right\} = 0. \end{cases} \tag{23}$$

According to the above calculation, the TET (18) is straight and easy to implement by the criterion (20). The entire procedure of the TET is summarized in Algorithm 1.

Algorithm 1 TET algorithm

1: Input the signal f, the window g, and the threshold τ, parameters C_ω, C_β;

2: Let $Te = \vec{0}$, a zero matrix;

3: Calculate the $\tilde{\omega}(t,\omega,\beta)$ and the $\tilde{\beta}(t,\omega,\beta)$ from (23);

4: For the point (t,ω,β) satisfying (20), i.e.,

$$\exp(-{C_\omega}^2\hat{\omega}(t,\omega,\beta)^2)\exp(-{C_\beta}^2\hat{\beta}(t,\omega,\beta)^2) > \tau,$$

then $Te(t,\omega,\beta) = C_f^g(t,\omega,\beta)$;

5: Output $Te(t,\omega,\beta)$.

The computational cost of the TET mainly focuses on the CT (i.e., C_f^g, C_f^{tg}, and $C_f^{t^2g}$) and extracting operations (i.e., Equation (20)). Assuming that a signal of N samples is utilized, and the number of the discrete β is N_β. The CT requires $O(N_\beta N^2\log_2 N)$ operations, and the extracting detection requires $O(N_\beta N^2)$ operations. Therefore, the total computing complexity of the TET is no more than $O(N_\beta N^2\log_2 N)$.

3.3. Signal reconstruction

According to (13), we can obtain that

$$C_f^g(t,\omega,\beta) \approx f(t)\sqrt{\sigma}\sqrt{\frac{2\pi}{1+j\sigma^2(\beta-\phi''(t))}}\exp(-\frac{\sigma^2(\omega-\phi'(t))^2}{2(1+j\sigma^2(\beta-\phi''(t)))}).$$

Evaluating the TET along the $(t,\phi'(t),\phi''(t))$, we have

$$Te(t,\phi'(t),\phi''(t)) = C_f^g(t,\phi'(t),\phi''(t)) \approx f(t)\hat{g}(0), \tag{24}$$

where $\hat{g}(\omega)$ is the Fourier transform of the window $g(t)$. Therefore, the original signal $f(t)$ can be estimated by its TET on the three-dimensional ridge, i.e.,

$$f(t) \approx \frac{Te(t,\phi'(t),\phi''(t))}{\hat{g}(0)}. \tag{25}$$

From (25), it is interesting to note that the CR of the signal contributes to the signal reconstruction, and this TET reconstruction extends the classic TF ridge reconstruction (see Theorem 4.6 in [61]) to three-dimension representation.

The difference of the CT between the second-order approximation and the true representation is bounded by the following lemma.

Lemma 1. *Suppose that* $f(t)$ *satisfies* $A(t) \in C^2(R) \cap L^\infty(R)$, $\phi(t) \in C^3(R)$, $\sup_{t\in R} \mid \phi'(t) \mid < \infty$, $\sup_{t\in R} \mid \phi''(t) \mid < \infty$, $\mid A''(t) \mid < \varepsilon$, *and* $\mid \phi'''(t) \mid < \varepsilon$, *then we have*

$$\mid C_f^g(t,\omega,\beta) - f(t)\sqrt{\sigma}\sqrt{\frac{2\pi}{1+j\sigma^2(\beta-\phi''(t))}}\exp(-\frac{\sigma^2(\omega-\phi'(t))^2}{2(1+j\sigma^2(\beta-\phi''(t)))}) \mid \leq \varepsilon\Gamma(t), \tag{26}$$

where $\varepsilon > 0$, $\Gamma(t) = \frac{1}{2}I_1 + \frac{1}{6}I_3(t)$, $I_n = \int_{-\infty}^{+\infty} \mid t \mid^n g(t)dt$.

Proof Since

$$\begin{aligned}
&\mid C_f^g(t,\omega,\beta) - f(t)\sqrt{\sigma}\sqrt{\frac{2\pi}{1+j\sigma^2(\beta-\phi''(t))}}\exp(-\frac{\sigma^2(\omega-\phi'(t))^2}{2(1+j\sigma^2(\beta-\phi''(t)))}) \mid \\
=&\mid C_f^g(t,\omega,\beta) - A(t)e^{j\phi(t)}\int_{-\infty}^{+\infty} g(\mu)e^{j(\frac{\phi''(t)}{2}\mu^2+\phi'(t)\mu)}e^{-j\frac{\beta\mu^2}{2}}e^{-j\omega\mu}d\mu \mid \\
\leq&\mid \int_{-\infty}^{+\infty} g(\mu)(A(\mu+t)-A(t))e^{j\phi(\mu+t)}e^{-j\frac{\beta\mu^2}{2}}e^{-j\omega\mu}d\mu \mid \\
&+ A(t) \mid \int_{-\infty}^{+\infty} g(\mu)(e^{j(\phi(\mu+t)-\phi(t)-\phi'(t)\mu-1/2\phi''(t)\mu^2}-1)e^{-j\frac{\beta\mu^2}{2}}e^{-j\omega\mu}d\mu \mid .
\end{aligned}$$

Under the assumption, we have $\mid A(\mu+t)-A(t) \mid \leq \varepsilon \mid \mu \mid$, then

$$\mid \int_{-\infty}^{+\infty} g(\mu)(A(\mu+t)-A(t))e^{j\phi(\mu+t)}e^{\frac{-j\beta\mu^2}{2}}e^{-j\omega\mu}d\mu \mid \leq \varepsilon\int_{-\infty}^{+\infty} \mid \mu \mid g(\mu)d\mu$$

Due to that $\mid \exp(j(\phi(\mu+t)-\phi(t)-\phi'(t)\mu-1/2\phi''(t)\mu^2))) - 1 \mid \leq \frac{\varepsilon}{6}\mu^3$, then

$$A(t) \mid \int_{-\infty}^{+\infty} g(\mu)e^{j(\phi(\mu+t)-\phi(t)-\phi'(t)\mu-1/2\phi''(t)\mu^2}e^{-j\frac{\beta\mu^2}{2}}e^{-j\omega\mu}d\mu \mid \leq \frac{\varepsilon}{6}A(t)\int_{-\infty}^{+\infty} \mid \mu \mid^3 g(\mu)d\mu,$$

which finishes the proof.

Based on Lemma 1, one can easily get the following theorem, which gives a mathematical proof for the performance of the TET reconstruction (25).

Theorem 3. *Suppose that $f(t)$ satisfies the conditions in the statement of Lemma 1, then there exists a constant C such that*

$$| \frac{Te(t, \phi'(t), \phi''(t))}{\hat{g}(0)} - f(t) | \leq C\varepsilon. \tag{27}$$

4. Numerical validation

In this section, the proposed TET method is tested on several simulation signals. In order to clearly illustrate the TET result, we employ the spectral clustering (SC) algorithm [62] to extract each component from the TET representation.

The parameters of the TET should be chosen appropriately. Generally, the optimal value of γ is strongly related to the noise level of the signal and the input of window length. In our experiments, the hard threshold method as used in [25,42] is employed to select parameter γ. The parameter analysis for C_ω and C_β is discussed in Section 4.3. The parameter τ in (20) is taken as $\tau = 0.3$ (for the test (10)) and $\tau = 0.8$ (for the test (28)) in this paper.

4.1. Crossed multi-component signals detection

The first test is to consider the performance of the TET in detecting the crossed signal (10). Fig. 4 presents the clustering results of the TET representation. From Fig. 4, we can see that, the TET achieves a high concentration TFCR representation, successfully characterizes the feature of the overlapped signal in the TFCR domain and obtains a good IFs estimation. However, it is difficult to separate the crossed signal from the TF domain or the time-CR domain due to the interference of different modes. It is noted that a error exists in the CR estimation for the TET, but it still plays a critical role in three-dimensional representation because the CR contributes to a more accurate IF estimation especially for the overlapped signals.

For comparison, the results obtained by two classic TF post-processing methods, i.e., the SST [25] and RM [16], are displayed in Fig. 5, where Fig. 5(c,d) shows the estimated IFs by the ridge detection algorithm [63]. It can be seen from the results that the SST and RM methods generate an inaccurate estimation for IFs in the TF domain, and easily leading to the mixture of different modes. In addition, the computational times required for the TET, SST and RM in addressing the signal (10) are 4.571 s, 0.076 s, and 0.078 s respectively (the tested computer configuration: Intel Core i5-6600 3.30 GHz, 8.0 GB of RAM, and MATLAB version R2018b). Inevitably, addressing the multi-component signal in three-dimensional space increases the calculation. More efficient implementation of the TET needs to consider.

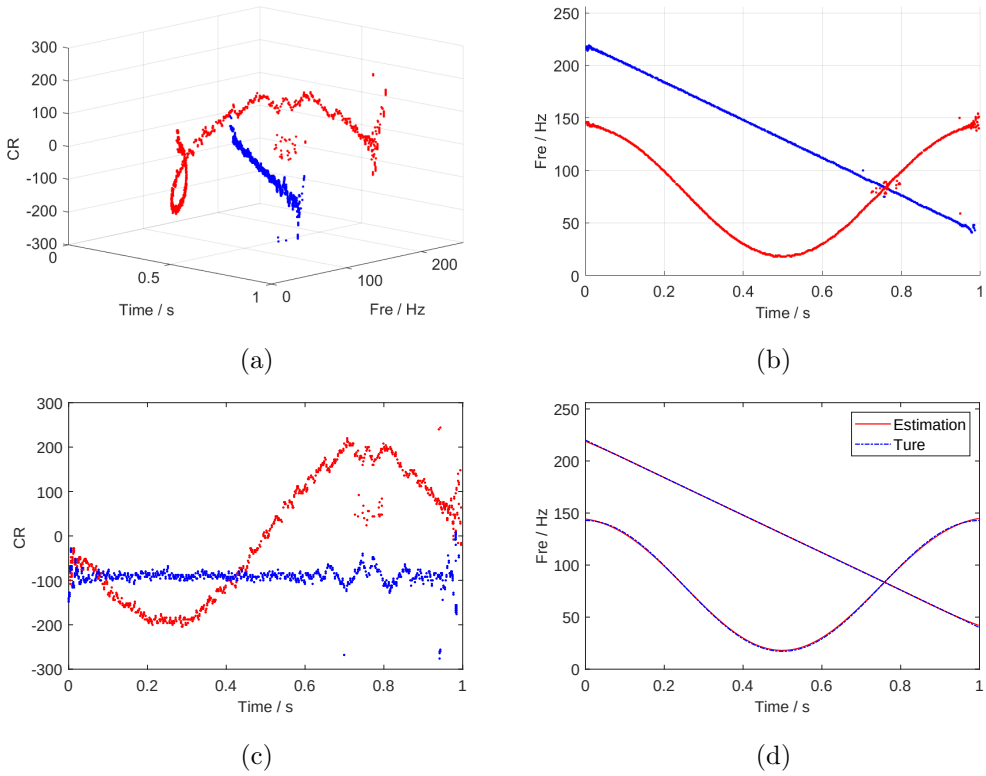

Figure 4: The TET results. (a) The TFCR of TET, (b) TF plot of TET, (c) time-CR plot of TET, (d) the estimated IFs by TET.

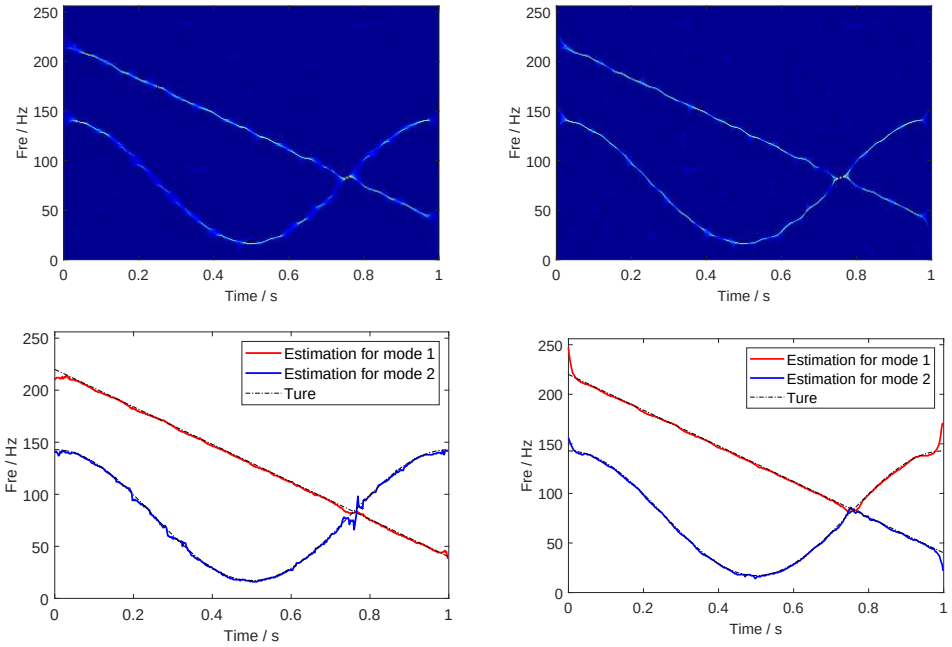

Figure 5: The SST result and RM result (top), the detected IF by SST and RM (bottom).

Furthermore, we test the reconstruction performance of the TET compared with the SST method (ds =10, where ds denotes the reconstruction bandwidth). The reconstruction results of the signal (10)

are displayed in Fig. 6. It can be found that, both of two methods successfully recover the separated part of the signal. The overlapped part obtained by the TET is much closer to the original signal than that of the SST. Indeed, compared with the SST method, the merits of the TET is that, it can reduce the influence of the overlapping points, and the reconstruction region in the TET representation is smaller, which can introduce less noise into the reconstructed signal.

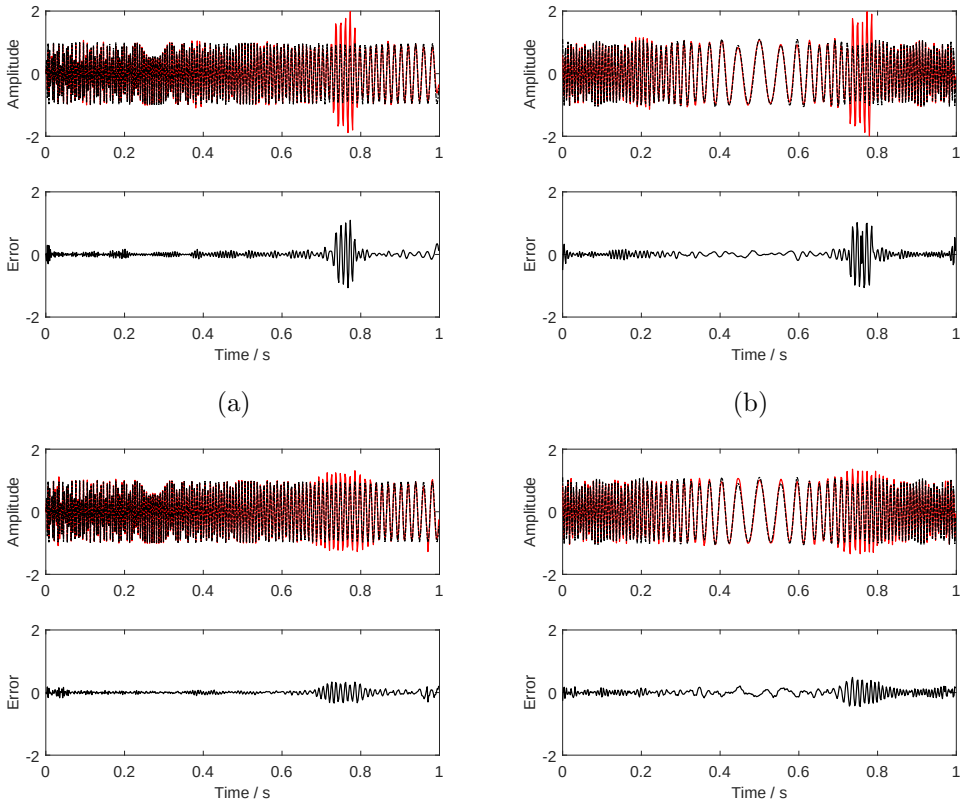

Figure 6: Reconstruction results for SST and TET. (a) The mode $f_1(t)$ recovered by SST, (b) the mode $f_2(t)$ recovered by SST, (c) the mode $f_1(t)$ recovered by TET, (d) the mode $f_2(t)$ recovered by TET, where the top row displays the original signal (black - -), the reconstructed signal (red -), the bottom row shows the reconstruction errors.

Next, let us consider a three-components AM-FM signal with small CR values as

$$\begin{aligned} f(t) &= f_1(t) + f_2(t) + f_3(t) + n(t), \\ f_1(t) &= \cos(2\pi \times (40t - 80\sin(0.5\pi t))), \\ f_2(t) &= \cos(2\pi \times (50t + 100\sin(0.5\pi t))), \\ f_3(t) &= (1 + 0.1\cos(0.6\pi t))\cos(2\pi \times (50t + 7t^2)), \end{aligned} \tag{28}$$

where $n(t)$ is a Gaussian noise with the SNR= 8 dB. The sampling frequency is 256 Hz, and time duration is [0 4].

Fig. 7 provides two slices of the CT and TET at $t = 1.168$ s and $t = 2.0$ s, where the red notes are the true instantaneous information of the signal. The results again prove that the proposed TET effectively sharpens the TFCR representation, obtaining a much more concentrated result than that of the CT. From the Fig. 7(c) and the clustered results presented in the Fig. 8(a,c), we can know that the TET sometimes yields error in locating the true CR. But this shortcoming has little influence on the IF estimation. It can be seen from the Fig. 7(c,d) and Fig. 8(b,d) that the TET achieves a good IFs detection, which in turn brings a perfect result for CR estimation because of the derivative relation between the IF and the CR. In addition, Fig. 9 displays the TF results obtained by the SST and RM methods. It can be observed that, in the TF plane around the cross point, there are heavy cross-terms between two modes, and the TF methods cannot characterize the true IF trajectories. By comparison, it shows that the proposed TET has clear advantages in addressing the overlapped multi-component signals even with small CRs.

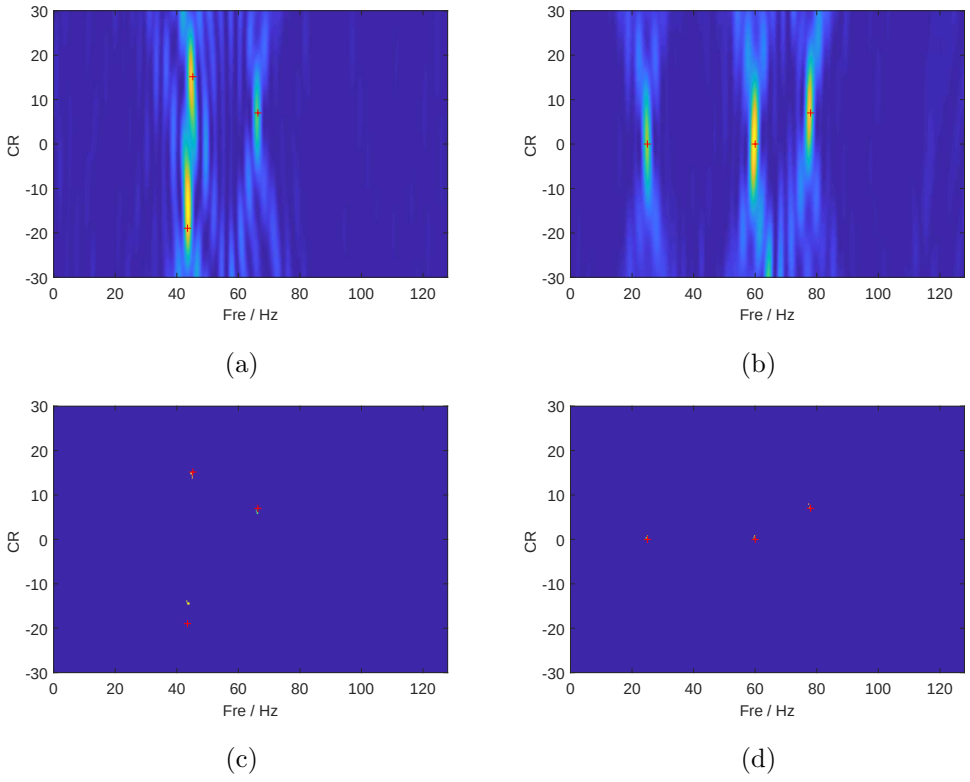

Figure 7: Frequency-CR plots by the CT and TET at different times. (a) The CT result at $t = 1.168$ s, (b) the CT result at $t = 2.0$ s, (c) the TET result at $t = 1.168$ s, (d) the TET result at $t = 2.0$ s.

4.2. Performance in robustness to noise

In order to explore the performance of the TET method in noise tolerance, in this section we give the IF estimates of the signal (10) under different noise levels. The SST and RM methods are also used for

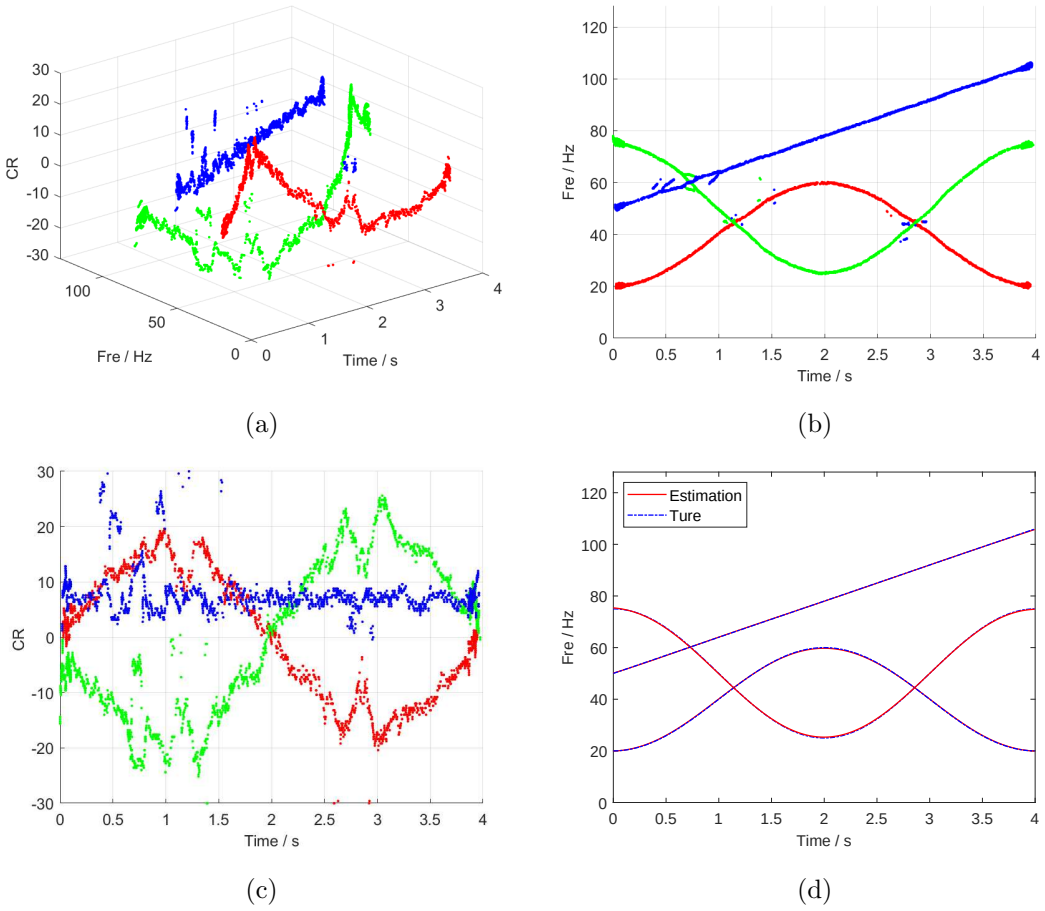

Figure 8: The detected results of the TET. (a) The TFCR representation by the TET and SC, (b) the TF plot of the TET, (c) the time-CR plot of the TET, (d) the IF estimation by the TET.

comparison. The detected result is evaluated by the mean square error (MSE) as follows

$$\mathrm{MSE} = \frac{1}{N} \parallel \widetilde{\mathrm{IF}} - \mathrm{IF} \parallel_2^2, \tag{29}$$

where N is the discrete length of the IF, $\| \cdot \|_2$ denotes l_2-norm, IF is the original clean IF, and $\widetilde{\mathrm{IF}}$ represents the estimated IF. The experiments are conducted by running 50 times and the average performance of the best 30 is recorded as the final result.

Fig. 10 shows the MSE values of the IF estimation by the SST, RM and TET when adding different noise. It can be seen that the IF estimation obtained by the TET is more accurate than that of the SST and RM for SNR$\geq$ 2. In the strong noise environment, the multi-component signal can not be effectively extracted by the three methods. In this regard, robust ridge detection instead of the SC algorithm for the TET should be considered in the future.

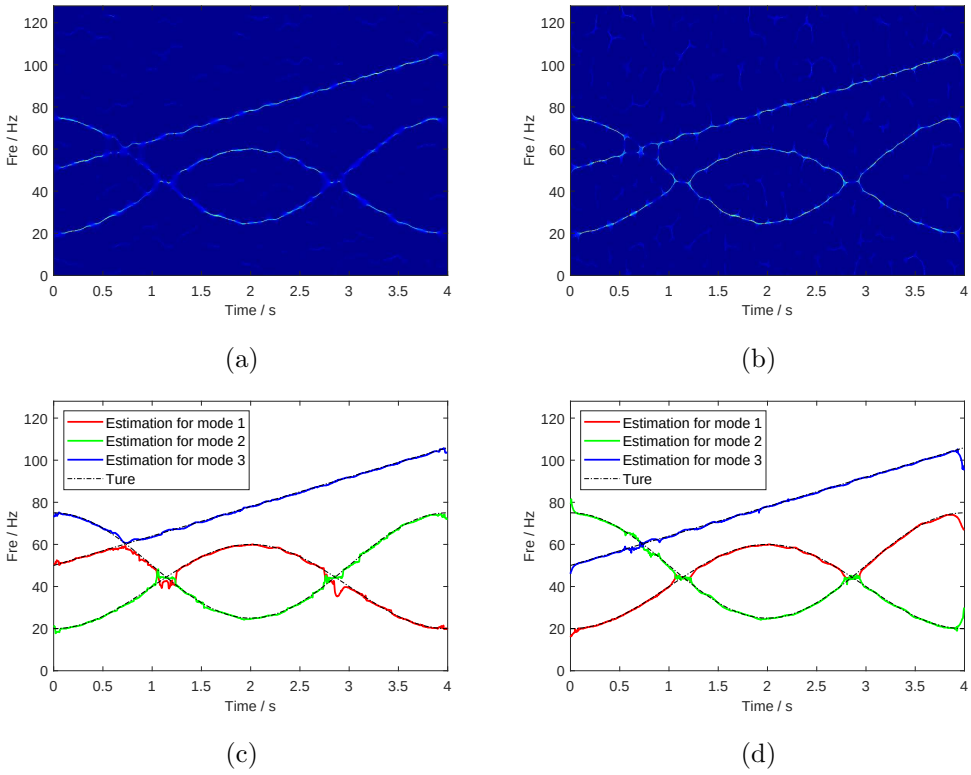

Figure 9: TF results of the SST and RM. (a) SST result, (b) RM result, (c) the detected IF by SST, (d) the detected IF by RM.

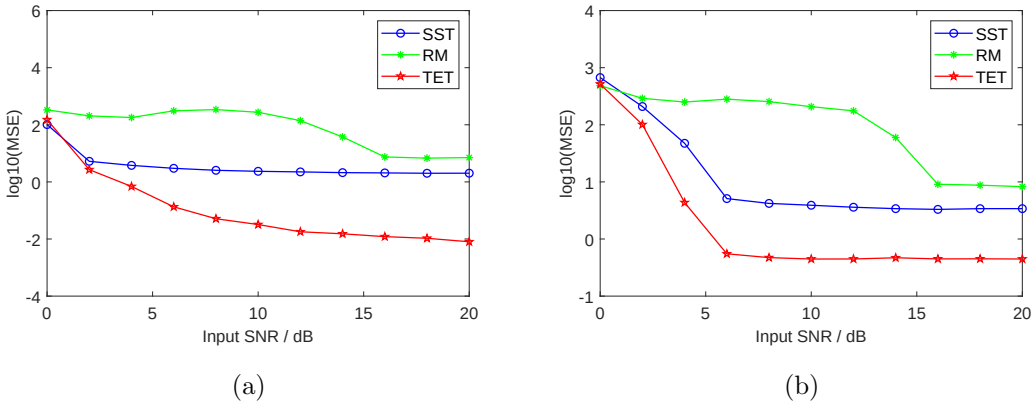

Figure 10: MSEs of the IF estimation under different SNRs. (a) The MSEs of $f_1(t)$, (b) the MSE of $f_2(t)$.

4.3. Parameters selection for C_ω and C_β

In this section we discuss the effect of the parameters C_ω and C_β on the TET and give their reference ranges. We employ the signals (10) and (28) under the SNR= 16 dB to test, and the IF estimates by the TET with different C_ω and C_β are shown in Fig. 11. From the results, we can know that there are various combinations of the two parameters (e.g., $C_\omega = 1000$, $C_\beta = 10$) can be chosen for the TET to address various multi-component signals. Too large values for these two parameters are undesirable, and

generally they are recommended as $C_\omega \in [200\ 1200]$, $C_\beta \in [10\ 30]$ in experiments.

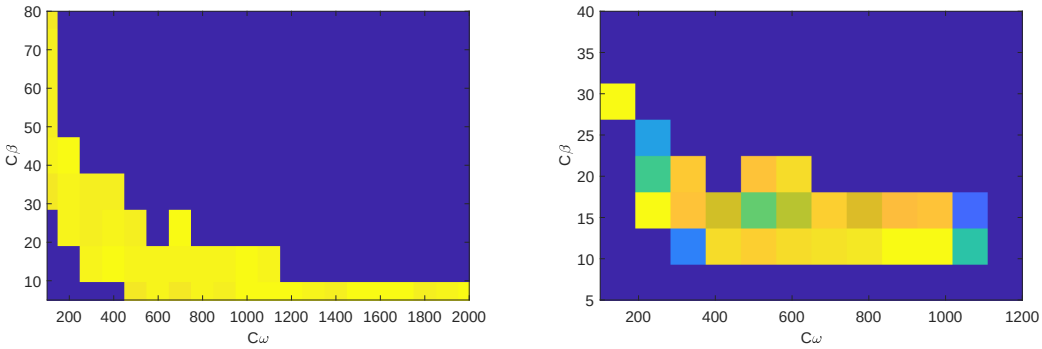

(a) (b)

Figure 11: MSEs of the IF estimation for different parameters. (a) The exp(−MSE) of the IF estimation of the signal (10), (b) the exp(−MSE) of the IF estimation of the signal (28).

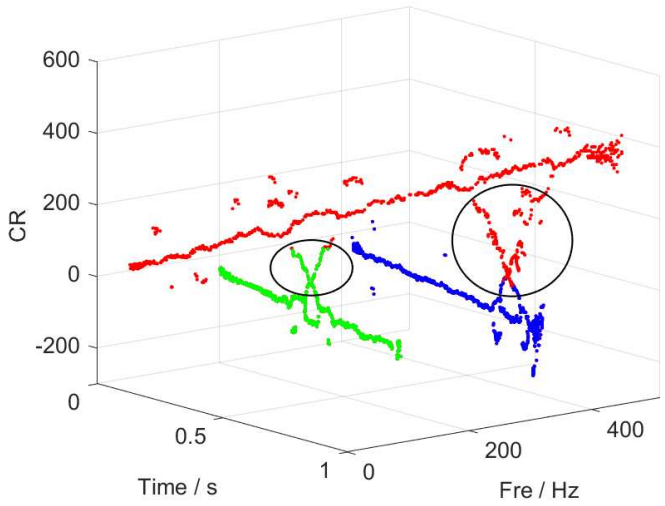

Figure 12: An illustration for the TET.

5. Conclusion and discussion

In this paper, three-dimensional extracting transform (TET) is presented to generate a concentrated TFCR representation for multi-component non-stationary signals. The TET can provide joint IF and CR estimation, making the TF crossed signals appear as separated in the TFCR domain, which effectively solves the separability limitation of the SST. Based on the chirplet transform, we derive the IF and CR equations and an exponential transform of that two equations is introduced to extract the IF and CR points in the three-dimensional space. By performing the spectral clustering algorithm on the detected TFCR points, the permutations between the intersected components in the TF plot are

solved. Experimental results illustrate that the TET obtain good component separation and perfect IF estimation.

Although the proposed method has a good performance in analyzing a wide range of multi-component signals, some works should be considered.

1) As presented in Fig. 12, the interference of different components still exists in the TFCR representation (see the elliptic region of the figure). This limitation is partly because of the effect of the CR variable β. Exploring more effective way, instead of the CR equation (16), to obtain a good estimate for CR is required.

2) The TET suffers from the intrinsic limitation that it operates on a linear chirplet transform. Indeed, a narrow window spreads the CT representation, which easily causes the interference of different modes.

3) How to effectively extract the ridges associated with the modes from the TET representation seems to be a better option than using clustering methods. Moreover, robust analysis of the TET and the application to real-life signals need to be further investigated.

Acknowledgements

This work was partially supported by the Major Research Plan of the National Natural Science Foundation of China under grant no. 91730306 and the National Key R and D Program of the Ministry of Science and Technology of China under Grant no. 2018YFC0603501.

References

[1] S. Fomel, Seismic data decomposition into spectral components using regularized nonstationary autoregression, Geophysics 78 (6) (2013) O69-O76.

[2] N. Liu, J. Gao, B. Zhang, Q. Wang, X. Jiang, Self-adaptive generalized S-transform and its application in seismic time-frequency analysis, IEEE Trans. Geosci. Remote Sens. 57 (10) (2019) 7849-7859.

[3] S. Liu, T. Shan, Y.D. Zhang, Detection of weak astronomical signals with frequency-hopping interference suppression, Dig. Signal Process. 72 (2018) 1-8.

[4] L. Cohen, Time-Frequency Analysis, Prentice-Hall, Englewood Cliffs, NJ, 1995.

[5] M.G. Amin, Y.D. Zhang, F. Ahmad, K. Ho, Radar signal processing for elderly fall detection: The future for in-home monitoring, IEEE Signal Process. Mag. 33 (2) (2016) 71-80.

[6] C. Park, D. Looney, P. Kidmose, M. Ungstrup, D.P. Mandic, Time-frequency analysis of EEG asymmetry using bivariate empirical mode decomposition, IEEE Trans. Neural Syst. Rehabil. Eng. 19 (4) (2011) 366-373.

[7] H. Yang, Synchrosqueezed wave packet transforms and diffeomorphism based spectral analysis for 1D general mode decompositions, Appl. Computat. Harmon. Anal. 39 (1) (2015) 33-66.

[8] X. Zhu, Z. Zhang, J. Gao, W. Li, Two robust approaches to multicomponent signal reconstruction from STFT ridges, Mech. Syst. Signal Process. 115 (2019) 720-735.

[9] B. Liu, S.D. Riemenschneider, Y.S. Xu, Gearbox fault diagnosis using empirical mode decomposition and Hilbert spectrum, Mech. Syst. Signal Process. 20 (3) (2006) 718-734.

[10] M.R. Portnoff, Time-frequency representation of digital signals and systems based on short-time Fourier analysis, IEEE Trans. Acoust. Speech Signal Process. 28 (1) (1980) 55-69.

[11] A. Grossmann, J. Morlet, Decomposition of hardy functions into square integrable wavelets of constant shape, SIAM J. Math. Anal. 15 (4) (1984) 723-736.

[12] T. Claasen, W. Mecklenbräuker, The Wigner distribution-A tool for time-frequency signal analysis-Part I: Continuous-time signals, Philips J. Res. 35 (1980) 217-250.

[13] F. Hlawatsch, G.F. Boudreaux-Bartels, Linear and quadratic time-frequency signal representations, IEEE Signal Process. Mag. 9 (2) (1992) 21-67.

[14] D. Jones, R.G. Baraniuk, An adaptive optimal-kernel time-frequency representation, IEEE Trans. Signal Process. 43 (10) (1995) 2361-2371.

[15] K. Kodera, R. Gendrin, C. Villedary, Analysis of time-varying signals with small BT values, IEEE Trans. Acoust. Speech Signal Process. 26 (1978) 64-76.

[16] F. Auger, P. Flandrin, Improving the readability of time-frequency and time-scale representations by the reassignment method, IEEE Trans. Signal Process. 43 (5) (1995) 1068-1089.

[17] F. Auger, P. Flandrin, Y. Lin, S. McLaughlin, S. Meignen, T. Oberlin, H.T. Wu, Time-frequency reassignment and synchrosqueezing: an overview, IEEE Signal Process. Mag. 30 (6) (2013) 32-41.

[18] S. Meignen, T. Oberlin, D.H. Pham, Synchrosqueezing transforms: From low- to high-frequency modulations and perspectives, C. R. Phys. 20 (2019) 449-460.

[19] N.E. Huang, Z. Shen, S.R. Long, M. Wu, H. Shih, Q. Zheng, N. Yen, C. Tung, H. Liu, The empirical mode decomposition and Hilbert spectrum for nonlinear and nonstationary time series analysis, Proc. R. Soc. Lond. A 454 (1998) 903-995.

[20] B.M. Battista, C.C. Knapp, T. McGee, V. Gobel, Application of the empirical mode decomposition and Hilbert-Huang transform to seismic reflection data, Geophysics 72 (2) (2007) H29-H37.

[21] B. Liu, S.D. Riemenschneider, Y.S. Xu, Gearbox fault diagnosis using empirical mode decomposition and Hilbert spectrum, Mech. Syst. Signal Process. 20 (3) (2006) 718-734.

[22] G. Rilling, P. Flandrin, One or two frequencies? The empirical mode decomposition answers, IEEE Trans. Signal Process. 56 (1) (2008) 85-95.

[23] D.P. Mandic, R.U. Rehman, Z. Wu, N.E. Huang, Empirical mode decomposition-based time-frequency analysis of multivariate signals: the power of adaptive data analysis, IEEE Signal Process. Mag. 30 (6) (2013) 74-86.

[24] I. Daubechies, S. Maes, A nonlinear squeezing of the continuous wavelet transform based on auditory nerve models, in: Wavelets in Medicine and Biology, CRC Press, 1996, pp. 527-546.

[25] I. Daubechies, J.F. Lu, H.T. Wu, Synchrosqueezed wavelet transforms: an empirical mode decomposition-like tool, Appl. Computat. Harmon. Anal. 30 (2011) 243-261.

[26] G. Thakur, H.T. Wu, Synchrosqueezing-based recovery of instantaneous frequency from nonuniform samples, SIAM J. Math. Anal. 43 (5) (2012) 2078-2095.

[27] H. Yang, L. Ying, Synchrosqueezed curvelet transform for two dimensional mode decomposition, SIAM. J. Math. Anal. 46 (3) (2014) 2052-2083.

[28] H. Yang, L. Ying, Synchrosqueezed wave packet transform for 2D mode decomposition, SIAM J. Imaging Sci. 6 (2013) 1979-2009.

[29] Z. Huang, J. Zhang, Z. Zou, Synchrosqueezing S-transform and its application in seismic spectral decomposition, IEEE Trans. Geosci. Remote Sens. 54 (2) (2016) 817-825.

[30] X. Zhu, Z. Zhang, Z. Li, J. Gao, X. Huang, G. Wen, Multiple squeezes from adaptive chirplet transform, Signal Process. 163 (2019) 26-40.

[31] G. Thakur, E. Brevdo, N.S. Fučkar, H.T. Wu, The Synchrosqueezing algorithm for time-varying spectral analysis: Robustness properties and new paleoclimate applications, Signal Process. 93 (2013) 1079-1094.

[32] I. Daubechies, Y. Wang, H.T. Wu, ConceFT: concentration of frequency and time via a multitapered synchrosqueezed transform, Philos. Trans. R. Soc. 374 (2065) (2016) 20150193.

[33] H. Yang, Statistical analysis of synchrosqueezed transforms, Appl. Computat. Harmon. Anal. 45 (3) (2018) 526-550.

[34] A. Ahrabian, D. Looney, L. Stanković, D.P. Mandic, Synchrosqueezing-based time-frequency analysis of multivariate data, Signal Process. 106 (2015) 331-341.

[35] L. Stanković, D. Mandić, M. Daković, M. Brajović, Time-frequency decomposition of multivariate multicomponent signals, Signal Process. 142 (2018) 468-479.

[36] C. Li, M. Liang, A generalized synchrosqueezing transform for enhancing signal time-frequency representation, Signal Process. 92 (2012) 2264-2274.

[37] T. Oberlin, S. Meignen, V. Perrier, Second-order synchrosqueezing transform or invertible reassignment? Towards ideal time-frequency representations, IEEE Trans. Signal Process. 63 (2015) 1335-1344.

[38] S. Wang, X. Chen, G. Cai, B. Chen, X. Li, Z. He, Matching demodulation transform and synchrosqueezing in time-frequency analysis, IEEE Trans. Signal Process. 62 (1) (2014) 69-84.

[39] D.H. Pham, S. Meignen, High-order synchrosqueezing transform for multicomponent signals analysis-with an application to gravitational-wave signal, IEEE Trans. Signal Process. 65 (12) (2017) 3168-3178.

[40] G. Yu, Z. Wang, P. Zhao, Multi-synchrosqueezing transform, IEEE Trans. Ind. Electron. 66 (7) (2019) 5441-5455.

[41] D. He, H. Cao, S. Wang, X. Chen, Time-reassigned synchrosqueezing transform: The algorithm and its applications in mechanical signal processing, Mech. Syst. Signal Process. 117 (2019) 255-279.

[42] G. Yu, M. Yu, C. Xu, Synchroextracting transform, IEEE Trans. Ind. Electron. 64 (10) (2017) 8042-8054.

[43] X. Zhu, Z. Zhang, J. Gao, B. Li, Z. Li, X. Huang, G. Wen, Synchroextracting chirplet transform for accurate IF estimate and perfect signal reconstruction, Dig. Signal Process. 93 (2019) 172-186.

[44] M. Aoi, K. Lepage, Y. Lim, U.T. Eden, T.J. Gardner, An approach to time-frequency analysis with ridges of the continuous chirplet transform, IEEE Trans. Signal Process. 63 (3) (2015) 699-710.

[45] Z. Li, J. Gao, Z. Wang, A time-synchroextracting transform for the time-frequency analysis of seismic data, IEEE Geosci. Remote Sens. Lett., 2019, doi: 10.1109/LGRS.2019.2931138.

[46] K. Fitz, L. Haken, On the use of time frequency reassignment in additive sound modeling, J. Audio Eng. Soc. 50 (11) (2002) 879-893.

[47] V. Bruni, M. Tartaglione, D. Vitulano, On the time-frequency reassignment of interfering modes in multicomponent fm signals, in: Proc. 26th European Signal Processing Conference (EUSIPCO), Rome, 2018, pp.722-726.

[48] V. Bruni, M. Tartaglione, D. Vitulano, An iterative approach for spectrogram reassignment of frequency modulated multicomponent signals, Math. Comput. Simulat., 2019, doi: https://doi.org/10.1016/j.matcom.2019.11.006.

[49] S. Chen, X. Dong, G. Xing, Z. Peng, W. Zhang, G. Meng, Separation of overlapped non-stationary signals by ridge path regrouping and intrinsic chirp component decomposition, IEEE Sensors J. 17 (18) (2017) 5994-6005.

[50] P. Li, Q. Zhang, IF estimation of overlapped multicomponent signals based on viterbi algorithm, Circuits Syst. Signal Process., 2019, doi: 10.1007/s00034-019-01314-8.

[51] B. Porat, B. Friedlander, Asymptotic statistical analysis of the high order ambiguity function for parameter estimation of polynomial-phase signals, IEEE Trans. Inform. Theor. 42 (3) (1996) 995-1001.

[52] S. Barbarossa, A. Scaglione, and G.B.Giannakis, Product high-order ambiguity function for multicomponent polynomial-phase signal modeling, IEEE Trans. Signal Process. 46 (3) (1998) 691-708.

[53] P. O'Shea, A new technique for instantaneous frequency rate estimation, IEEE Signal Process. Lett. 9 (8) (2002) 251-252.

[54] I. Djurovic, M. Simeunovic, P. Wang, Cubic phase function: A simple solution to polynomial phase signal analysis, Signal Process. 135 (2017) 48-66.

[55] S. Mann, S. Haykin, The chirplet transform: physical considerations, IEEE Trans. Signal Process. 43 (11) (1995) 2745-2761.

[56] F. Tian, Y. Yang, L. Xu, Doppler parameters estimation by short time chirp Fourier transform, IEEE International Conference on Signal Processing, Communications and Computing (ICSPCC), Xi¡an, 2011, pp. 76-81.

[57] G. Yu, Y. Zhou, General linear chirplet transform, Mech. Syst. Signal Process. 70-71 (2016) 958-973.

[58] X. Zhu, Z. Zhang, H. Zhang, J. Gao, B. Li, Generalized ridge reconstruction approaches toward more accurate signal estimate, Circuits Syst. Signal Process. 2019, doi: https://doi.org/10.1007/s00034-019-01278-9.

[59] E.J. Candes, P.R. Charlton, H. Helgason, Detecting highly oscillatory signals by chirplet path pursuit, Appl. Comput. Harmon. Anal. 24 (1) (2008) 14-40.

[60] W. Zhang, Y. Fu, Y. Li, Sparse time-frequency-frequency-rate representation for multicomponent nonstationary signal analysis, in: Proc. 26th European Signal Processing Conference (EUSIPCO), Rome, 2018, pp. 717-721.

[61] S. Mallat, A Wavelet Tour of Signal Processing: The Sparse Way (3rd edn), Academic Press, Burlington, 2009.

[62] W. Chen, Y. Song, H. Bai, C. Lin, E. Chang, Parallel spectral clustering in distributed systems, IEEE Trans. Pattern. Anal. Mach. Intell. 33 (3) (2011) 568-586.

[63] S. Meignen, D.H. Pham, S. McLaughlin, On demodulation, ridge detection and synchrosqueezing for multicomponent signals, IEEE Trans. Signal Process. 65 (8) (2017) 2093-2103.